Journal of Materials Chemistry B

RSC Publishing

COMMUNICATION

View Article Online
View Journal | View Issue

Cite this: *J. Mater. Chem. B*, 2013, **1**, 5393

Received 26th June 2013
Accepted 14th August 2013

DOI: 10.1039/c3tb20899k

www.rsc.org/MaterialsB

BSA–rGO nanocomposite hydrogel formed by UV polymerization and *in situ* reduction applied as biosensor electrode†

Zhou Tang,[a] Lu Gao,[a] Yihua Wu,[b] Teng Su,[a] Qing Wu,[a] Xinhua Liu,[a] Wenjun Li*[a] and Qigang Wang*[ac]

This communication demonstrates a convenient strategy to prepare a tough BSA–rGO hydrogel electrode *via* photopolymerization, which is demonstrated to be a highly effective H_2O_2 biosensor electrode with low detection concentration and high sensing sensitivity after combining with hemin chloride.

Graphene oxide (GO) is the most significant chemical derivative of graphene, which has attracted great attention due to its easy and cost-effective preparation.[1] For achieving better electronic performance, GO should be changed to the reduced graphene oxide (rGO) form.[2] As electrode materials for biosensors, the direct use of rGO does not significantly prevent the restacking of single sheets. This is one of the most important problems that needs to be addressed before they can be used in a large-scale manner. Therefore, free-standing rGO hydrogel electrodes comprising highly dispersed rGO are highly needed, which have open channels for unobstructed transportation of detecting substances. In general, the mild combination of GO into hydrogels is easy to be realized *via* the traditional hydrogelation. GO hybrid hydrogels can also be formed by the mild supramolecular forces between GO and various biomolecules.[3] The preparation of rGO hydrogels from a previous GO hydrogel requires the further hydrazine reduction[4] or hydrothermal treatment.[5] Shi *et al.* have reported a one-step hydrothermal reduction to obtain rGO hydrogel from GO aqueous dispersion.[6] Inspired by these pioneering works, we try to realize the one-step preparation of rGO hydrogel *via* a mild and facile approach.

Here, we employ a photopolymerization method to prepare bovine serum albumin (BSA) cross-linked polymer hydrogel,[7] which can adsorb and reduce the GO nanosheets *in situ* during irradiation. The adsorption ability of bovine serum albumin have been previously demonstrated by Liu *et al.* The tyrosine residues of BSA mainly contribute to the formation of rGO during the UV irradiation and polymerization.[8] In our work, the cooperative effect of the reductive surface groups around BSA and UV irradiation allows us to obtain rGO within the hydrogel under mild conditions. This novel one-step synthesis of BSA–rGO hydrogel provides greater flexibility than that prepared by the traditional hydrothermal method.

Our system employs three substances as its main structural components: GO, BSA, and *N*,*N*-dimethylacrylamide (DMAA). GO was prepared according to the Hummers method, which has been reported elsewhere, and DMAA is a water-soluble acrylamide derivative and its polymer (PDMAA) exhibits good stability against hydrolysis. BSA was acryloylated by reaction with *N*-acryloxysuccinimide (NAS) to generate vinyl groups. 2,2-Diethoxyacetophenone (DEAP) is a highly effective cleavage photoinitiator with non-yellowing residue and a high treating rate. The selected UV irradiation approach with photoinitiators can realize spatial/temporal control and mild curing relative to the traditional preparation of most hydrogels. Many research groups including our group have employed this method to facilely fabricate tough nanocomposite hydrogels at room temperature.

As shown in Fig. 1a and d, an aqueous mixture of GO, acryloylated BSA and DMAA is taken as the precursor. GO can be adsorbed onto the surface of BSA *via* hydrogen bonding (Fig. 1b). UV light irradiation can form free radicals by the cleavage of 2,2-diethoxyacetophenone (approx. 1% of monomer amount). The radical co-polymerization of DMAA and vinylated BSA generates a three-dimensional hydrogel, where the latter acts as cross-linkers. Accompanying with UV irradiated gelation, the adsorbed GO was reduced to rGO by the reductive groups around the BSA surface (Fig. 1c and e). A typical procedure of BSA–rGO–H is listed as follows. The brown aqueous

[a]*Department of Chemistry, Tongji University, Siping Road 1239, Shanghai 200092, P. R. China. E-mail: wangqg66@tongji.edu.cn; wjli@tongji.edu.cn; Fax: +86-21-65981097; Tel: +86-21-65989301*

[b]*School of Urban Development and Environmental Engineering, Shanghai Second Polytechnic University, Jinhai Road 2360, Shanghai 201209, P. R. China*

[c]*Advanced Research Institute for basic science, Tongji University, Siping Road 1239, Shanghai 200092, P. R. China*

† Electronic supplementary information (ESI) available: Preparation and characterization of hydrogel and details of electrochemical analyses. See DOI: 10.1039/c3tb20899k

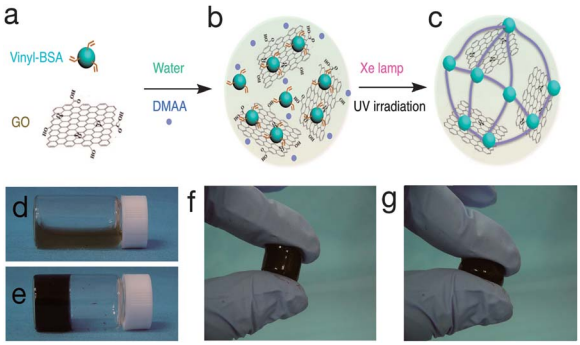

Fig. 1 Proposed scheme and optical images of the functional BSA–rGO–H. (a) The GO sheets, monomer, and Vinyl-BSA are homogeneously dispersed in water. (b) Then, Vinyl-BSA was linked onto the surface of the GO sheets. (c) Finally, the Vinyl-BSA was cross-linked to develop a 3D network. (d) Image of precursor 0.2 mg mL^{-1} GO sheets, monomer, and Vinyl-BSA, (e) image of the formed BSA–rGO–H. (f) Images of BSA–rGO–H. (g) Images of BSA–rGO–H with pressure.

mixture containing 0.02% (by mass) GO, 3.0% BSA (about 7.5% NAS relative to protein) and 5% DMAA (approx. 1% DEAP relative to monomer) with pH 7.0, changed into the black and tough BSA–rGO–H after 30 min UV irradiation (wavelength 365, intensity 20 mW cm^{-2}) at room temperature (approx. 25 °C). The final monomer conversion is higher than 98% by NMR measurements (Fig. S1, ESI†). Without the addition of GO, the same procedure gave the control hydrogel BSA–H with conversion above 98% after 20 min (Fig. S2, ESI†). The extended gelation time of samples with GO nanosheets may be due to their light-shielding effect.

The formation of rGO from GO in our BSA–rGO–H *via* hydrogelation can be confirmed by the variation of the relative intensities of G bands and D bands in their Raman spectra[10,11] (the E_{2g} mode of sp^2 carbon atoms and the symmetry A_{1g} mode). As shown in Fig. 2a, the intensity ratio of D/G bands increases after gelation, which agrees well with the Raman spectra of the reduced GO in the previous reports. Therefore, the GO in the hydrogel has been reduced to rGO during UV irradiation, which is in accordance with the color change from brown to black. The CV profiles of BSA–rGO–H modified GC electrode are detected in 0.5 M H_2SO_4 aqueous solution. As shown in Fig. S3 (ESI†), BSA–rGO–H has one pair of redox peaks with rectangular shape, which belongs to the typical transition between quinone/hydroquinone groups for rGO.[9] The control samples, *i.e.* BSA–H gel, single GO solution and their mixture, do not show these redox peaks.

The morphology of the lyophilized BSA–rGO–H hydrogel sample has been examined by scanning electron microscopy (SEM). As shown in Fig. 2b and c, the hydrogel has a well-defined and cross-linked 3D porous structure with 2–5 μm large pores and several hundred nanometer small pores. The TEM image (Fig. 2d) shows a series of well dispersed GO nanosheets in the final hydrogel, which arrange regularly to form a porous structure. The main difference between our rGO hydrogel and the tradition hydrothermal one is the role of rGO for the hydrogel fabrication. For our BSA–rGO nanocomposite hydrogel, the 0.02 wt% rGOs are not necessary for its network formation, although their presence can effectively reinforce the mechanical strength of hydrogels.

Our hydrogel is self-standing and able to sustain certain compression (Fig. 1f and g). The detailed mechanical analysis for a series of BSA–rGO–H hydrogels with various compositions are shown in Fig. 3 and Table 1. The compressive strength is selected as a collective index for the optimization of mechanical properties. For the hybrid gels with 3% BSA and 5% DMAA, the values of compressive strength increase from 62.43 kPa to 194.67 kPa and 124.83 kPa when the amount of GO increases from 0 to 0.02% and 0.04%, respectively (Fig. 3). The addition of GO can slightly increase the broken strain and Young's modulus by its reinforcement of hydrogel network *via* possible weak interaction with BSA and PDMAA. The further increase of GO with black color can hinder the UV light, which can lead to incomplete polymerization and low mechanical strength. Therefore, a GO content of 0.02% is optimal for the construction of tough BSA–rGO–H. For BSA–rGO–H with 0.02% GO and 5% DMAA, the value of compressive strength sharply decreases from 194.67 kPa to 107.70 kPa and 44.75 kPa when the amount of BSA increase from 3% to 5% and 7%, respectively. The optimized amount of BSA should be 3%, which is the minimum

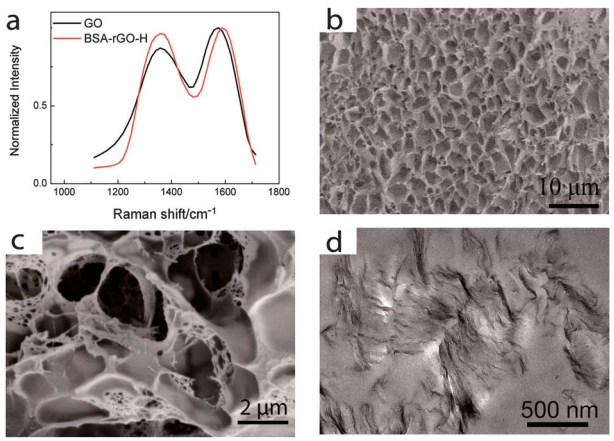

Fig. 2 Raman spectra (a) of BSA–rGO–H and GO. SEM images (b and c) of BSA–rGO–H and TEM image (d) of the BSA–rGO–H.

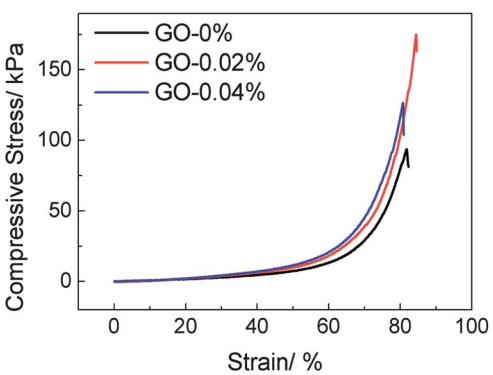

Fig. 3 Mechanical properties of BSA–rGO–H with different compositions. Compression properties of BSA–rGO–H containing 3% BSA, 5% DMAA and different GO concentrations.

Table 1 The mechanical properties of BSA–rGO–H with various compositions

No.	GO/BSA/DMAA (wt%)	Compressive strength (kPa)	Young's modulus (kPa)	Broken strain (%)
1	0/3/5	62.43 ± 2.11	6.72 ± 0.36	83.74 ± 1.73
2	0.02/3/3	11.16 ± 0.48	6.21 ± 0.33	58.70 ± 1.16
3	0.02/3/5	194.67 ± 9.47	6.88 ± 0.38	89.55 ± 2.82
4	0.02/3/7	92.04 ± 3.24	6.66 ± 0.35	84.35 ± 1.93
5	0.02/5/5	107.70 ± 3.66	16.53 ± 0.93	73.16 ± 1.78
6	0.02/7/5	44.75 ± 1.98	29.46 ± 1.52	55.14 ± 1.06
7	0.04/3/5	124.83 ± 5.06	6.98 ± 0.42	85.68 ± 1.44

concentration for complete gelation. In our BSA–rGO nanocomposite hydrogel, the acryloylated BSA act as crosslinking points of the network. Excessive BSA crosslinking points can cause the hydrogel to break easily at low strain and decrease the compressive strength. For BSA–rGO–H with 0.02% GO and 3% BSA, the value of compressive strength sharply increases from 11.16 kPa to 194.67 kPa and 92.04 kPa as the amount of DMAA increases from 3% to 5% and 7%, respectively. The increase of DMAA in the starting stage is helpful for the complete crosslinking between BSA. The further increase of DMAA can form a hydrogel with excessive crosslinking points, which can decrease its broken strain and therefore the compressive strength. The optimized amount of DMAA should be 5% for fabricating tough BSA–rGO–H. Therefore, the appropriate composition to form tough BSA–rGO–H should be 0.02% GO, 3% BSA and 5% DMAA, respectively.

A hydrogel, when applied as a biosensing platform, requires excellent conductivity. Therefore, we employed the AC impedance technique to detect the conductivity of BSA–rGO–H modified electrodes and various controls. The selected electrolyte was 0.1 M KCl containing 5 mM $Fe(CN)_6^{3-/4-}$ and the frequency range was between 1 Hz and 10 kHz, respectively. The curve fitting results (Fig. S4, ESI†) indicate that the charge-transfer resistance (R_{ct}) values of BSA–H modified electrode, BSA–H modified electrode soaking with GO, BSA–rGO–H modified electrode, and the naked GC electrode are 1477.6, 1460.7, 690.8, and 402.8 Ω, respectively. The conductivity of BSA–rGO–H modified electrode is about 2.1 times higher than those the BSA–H modified electrodes with/without GO. The excellent conductivity of BSA–rGO–H is beneficial to its application of as an electrode modifying material. Therefore, the peak current of BSA–rGO–H modified GC electrode is higher than that of BSA–H modified electrode with 5 mM $Fe(CN)_6^{3-/4-}$ as the active substance (Fig. S5, ESI†).

Here, we select hemin chloride, as the electron transfer mediator to measure the low H_2O_2 concentration. The loading of hemin molecules into BSA–rGO–H modified electrode are realized by the possible π–π stacking effect between the porphyrin ring of hemin and the atomic ring of GO.[10] After 24 hours incubation in the alkali solution of 1 mg mL^{-1} hemin, 0.45 mg hemin molecules can be adsorbed into the 25.7 mg BSA–rGO–H. The loaded amount of hemin within the BSA–rGO–H electrode was calculated by the change of the hemin concentration in solution before and after immersion, which can be measured by the UV-vis spectrum. The addition of hemin chloride to the BSA–rGO–H electrodes and controls have a negligible increase in their value of R_{ct} (Fig. S5, ESI†). The cyclic voltammetry (CV) curve of hemin/BSA–rGO–H modified electrode shows a clear reduction peak of hemin chloride at about −0.32 V (Fig. 4a). The stability of the modified electrode was investigated in N_2-saturated PBS (pH 6.88). As shown in Fig. 4a, only 12.8% decrease of the original reduction peak current is observed even after 100 cycles, which implies the considerable stability of the modified electrode. Fascinating is that this hemin/BSA–rGO–H modified electrode exhibits a very rapid recovery of its electrochemical performance after reloading in a fresh hemin alkali solution (Fig. 4b). Therefore, our BSA–rGO–H modified electrode is an effective platform to adsorb active hemin and functional proteins for biosensor applications, which can retain high stability and recover easily.

For fabricating the H_2O_2 sensor, the CV curves of the hemin/BSA–rGO–H electrode were measured with various H_2O_2

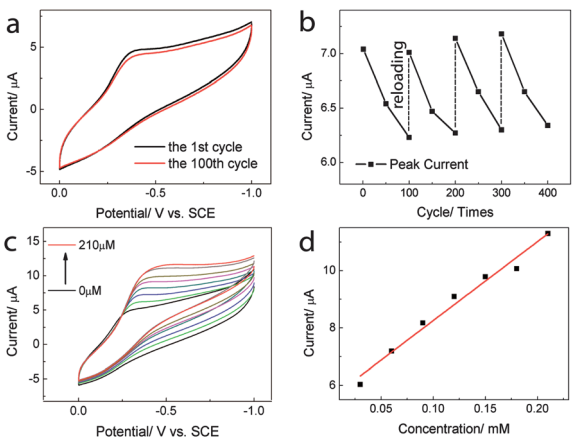

Fig. 4 Electrochemical properties of BSA–rGO–H modified electrode. (a) The first and 100th cycles of cyclic voltammograms of hemin/BSA–rGO–H modified electrode in 0.1 M PBS buffer saturated with N_2, scan rate 100 mV s^{-1}. Platinum sheet and saturated calomel electrode (SCE) were used as the counter and reference electrode, respectively. (b) Peak current of the cyclic voltammograms of hemin/BSA–rGO–H modified electrode in 0.1 M PBS buffer saturated with N_2, scan rate 100 mV s^{-1}. (c) Cyclic voltammograms of hemin/BSA–rGO–H modified electrode in 0.1 M PBS buffer before and after the addition of different amounts of H_2O_2 at a scan rate of 100 mV s^{-1}. The concentration increment of H_2O_2 for each step is 30 μmol L^{-1}. Platinum sheet and saturated calomel electrode (SCE) were used as the counter and reference electrode, respectively. (d) The linear fit of peak current to the concentration of H_2O_2.

concentrations (Fig. 4c). The nearly equal current steps for each addition of a controlled amount of H_2O_2 reflects the stable and efficient catalytic activity of the hydrogel sensor. A linear response of the current of the reduction peak to H_2O_2 concentration was obtained in the range of 0.03–0.21 mmol L^{-1} H_2O_2 (Fig. 4d). At the same time, the CV curves of the bare electrode and BSA–rGO–H electrode show no response to the various concentrations of H_2O_2 (Fig. S6 and S7, ESI†). According to the slope of this line, the sensing sensitivity was calculated to be 470.0 μA mM^{-1} cm^{-2}. The limit of detection, based on a signal-to-noise ratio of 3, is 1.04 μmol L^{-1}. The dynamic responses of the electrode with step by step adding of the H_2O_2 and with different H_2O_2 concentrations are shown in Fig. S8 and S9 (ESI).† The amperometric calibration curve is linear against the concentrations of H_2O_2 ranging from 0.35 mM to 9.5 mM, with a sensitivity of 86.5 μA mM^{-1} cm^{-2}. The current rises steeply to be stable in 8 ± 2 s, which suggests that the electron transfer process is a fast dynamic response. The static and dynamic sensitivity of our rGO hydrogel electrode are a little higher than that of the graphene directly modified electrodes.[10c,11] The main advantage of our rGO hydrogel electrodes relative to the existing graphene modified electrodes is their protective environment, which has excellent operative stability and can be completely reused easily after simple reloading.

In summary, we have demonstrated that UV polymerization offers a convenient and environmentally friendly strategy to prepare tough BSA–GH. The formation of rGO in the final hydrogels *via* the *in situ* reduction of BSA during gelation has been proven by Raman and electrochemical analysis. The further combination of hemin molecules with BSA–GH by π–π stacking can fabricate a H_2O_2 detecting electrode with sensing sensitivity as high as 470.0 μA mM^{-1} cm^{-2} and detecting limit as low as 1.04 μmol L^{-1}. The hybrid hydrogel is a promising biosensor platform due to the mild preparation, excellent mechanical strength, open channels and aqueous environment within them.

Experiment section

Preparation of hydrogel electrode

Graphite oxide was prepared by a modified Hummers method. Prior to use, the glass carbon (GC) electrode with 0.3 cm diameter was first polished with sand paper and chamois followed by 1.0 and 0.05 mm alumina slurry, then ultrasonically cleaned with double distilled water and ethanol, each for 10 min, and finally rinsed with double distilled water and dried under N_2. The cleaned GC electrode was continually scanned in 0.5 M sulfuric acid until steady voltammograms were established, and then rinsed with water. The various hydrogel electrodes were prepared as follow. The 0.025 mL precursor solution was firstly dropped to the surface of glass carbon electrode, then irradiated under UV light (2.0 mW cm^{-2} intensity at 365 nm) for about 30 min to form hydrogel modified electrode, finally lyophilized to obtain the porous and dried sample for the following detecting. The BSA–H modified electrode was prepared in the same way.

Characterizations

For SEM observations, the hydrogel was cut to a cube shape of about 2 × 2 × 2 mm^3. Then, the small piece of sample was soaped successively in 50% ethanol (15 min), 70% ethanol (15 min), 90% ethanol (15 min), 100% ethanol (15 min), a mixture of 1 : 1 ethanol and isoamyl acetate (30 min) and last in pure isoamyl acetate (30 min) to replace the water in hydrogel with isoamyl acetate. Finally, the treated sample was dried by the critical point method (Critical Point Dryer CPD, K850, Quorum) and observed by SEM (Hitachi S-4800) at a voltage of 3 kV. The TEM sample was observed by TEM (JEM-2010, JEOL) at an accelerating voltage of 120 kV. All proton NMR spectra were obtained using a Bruker 400 MHz NMR spectrometer. Raman spectra were recorded from 200 to 2000 cm^{-1} on a Renishaw 2000 Confocal Raman Microprobe (Renishaw Instruments, England) using a 514.5 nm argon ion laser.

The compressive stress–strain measurements were performed on gels using a tensile-compressive tester (FR-108B, Farui Co.). The cylindrical gel sample with the 13 mm diameter and 7 mm thickness was set on the lower plate and compressed by the upper plate which was connected to a load cell (500 N), at a strain rate of 5 mm min^{-1}. Cyclic voltammetry (CV) and AC impedance technique measurements were carried out on a CHI 660D electrochemical workstation. Platinum sheet and saturated calomel electrode (SCE) were used as the counter and reference electrode, respectively.

Acknowledgements

This work was supported by the National Natural Science Foundation of China (no. 21274111), the Program for New Century Excellent Talents in University of Ministry of Education of China (NECT-11-0386), the Fundamental Research Funds for Central Universities, the Pujiang talents program (no. 11PJ1409500), and the Recruitment Program of Global Experts.

Notes and references

1 (*a*) K. S. Novoselov, A. K. Geim, S. V. Morozov, D. Jiang, Y. Zhang, S. V. Dubonos, I. V. Grigorieva and A. A. Firsov, *Science*, 2004, **306**, 666–669; (*b*) C. Lee, X. Wei, J. W. Kysar and J. Hone, *Science*, 2008, **321**, 385–388; (*c*) M. J. Allen, V. C. Tung and R. B. Kaner, *Chem. Rev.*, 2010, **110**, 132–145.

2 (*a*) W. S. Hummers Jr and R. E. Offeman, *J. Am. Chem. Soc.*, 1958, **80**, 1339; (*b*) S. Park and R. S. Ruoff, *Nat. Nanotechnol.*, 2009, **4**, 217–224; (*c*) Z. Liu, J. T. Robinson, X. M. Sun and H. J. Dai, *J. Am. Chem. Soc.*, 2008, **130**, 10876–10877.

3 (*a*) Y. X. Xu, Q. O. Wu, Y. Q. Sun, H. Bai and G. Q. Shi, *ACS Nano*, 2010, **4**, 7358–7362; (*b*) F. Sharifi, R. Bauld, M. S. Ahmed and G. Fanchini, *Small*, 2012, **8**, 699–706; (*c*) C. C. Huang, H. Bai, C. Li and G. Q. Shi, *Chem. Commun.*, 2011, **47**, 4962–4964.

4 (*a*) S. Stankovich, D. A. Dikin, R. D. Piner, K. A. Kohlhaas, A. Kleinhammes, Y. Jia, Y. Wu, S. T. Nguyen and R. S. Ruoff, *Carbon*, 2007, **45**, 1558–1565; (*b*) J. L. Zhang,

H. J. Yang, G. X. Shen, P. Cheng, J. Y. Zhang and S. W. Guo, *Chem. Commun.*, 2010, **46**, 1112–1114.

5 H. A. Becerril, J. Mao, Z. Liu, R. M. Stoltenberg, Z. Bao and Y. Chen, *ACS Nano*, 2008, **2**, 463–470.

6 Y. X. Xu, K. X. Sheng, C. Li and G. Q. Shi, *ACS Nano*, 2010, **4**, 4324–4330.

7 (*a*) W. E. Hennink and C. F. van Nostrum, *Adv. Drug Delivery Rev.*, 2012, **64**, 223–236; (*b*) V. Hlady and J. Buijs, *Curr. Opin. Biotechnol.*, 1996, **7**, 72–77; (*c*) H. M. Wang, Y. Shi, L. Wang and Z. M. Yang, *Chem. Soc. Rev.*, 2013, **42**, 891–901; (*d*) Y. Gao, F. Zhao, Q. G. Wang, Y. Zhang and B. Xu, *Chem. Soc. Rev.*, 2010, **39**, 3425–3433; (*e*) Q. G. Wang, Z. M. Yang, L. Wang, M. L. Ma and B. Xu, *Chem. Commun.*, 2007, 1032–1034; (*f*) Z. M. Yang, G. L. Liang and B. Xu, *Acc. Chem. Res.*, 2008, **41**(2), 315–326; (*g*) L. Chen, T. O. McDonald and D. J. Adams, *RSC Adv.*, 2013, **3**, 8714–8720; (*h*) J. Raeburn, T. O. McDonald and D. J. Adams, *Chem. Commun.*, 2012, **48**, 9355–9357; (*i*) Q. G. Wang, J. L. Myna and T. Aida, *Nature*, 2010, **463**, 339–343; (*j*) D. Zhang, J. H. Yang, S. Bao, Q. S. Wu and Q. G. Wang, *Sci. Rep.*, 2013, **3**, 1399; (*k*) A. M. Tang, W. J. Wang, B. Mei, W. L. Hu, M. Wu and G. L. Liang, *Sci. Rep.*, 2013, **3**, 1848; (*l*) P. Vemula and G. John, *Acc. Chem. Res.*, 2008, **41**, 769–782; (*m*) P. Vemula, J. Li and G. John, *J. Am. Chem. Soc.*, 2006, **128**, 8932–8938; (*n*) J. Nanda, A. Biswas, B. Adhikari and A. Banerjee, *Angew. Chem., Int. Ed.*, 2013, **52**, 5041; (*o*) Y. C. Lai, *J. Appl. Polym. Sci.*, 1997, **66**, 1475–1484.

8 J. B. Liu, S. H. Fu, B. Yuan, Y. L. Li and Z. X. Deng, *J. Am. Chem. Soc.*, 2010, **132**, 7279–7281.

9 (*a*) Y. Chen, X. O. Zhang, D. C. Zhang, P. Yu and Y. W. Ma, *Carbon*, 2011, **49**, 573–580; (*b*) Y. Wang, Z. Q. Shi, Y. Huang, Y. F. Ma, C. Y. Wang, M. M. Chen and Y. S. Chen, *J. Phys. Chem. C*, 2009, **113**, 13103–13107.

10 (*a*) T. Xue, S. Jiang, Y. Q. Qu, Q. Su, R. Cheng, S. Dubin, C. Y. Chiu, R. Kaner, Y. Huang and X. F. Duan, *Angew. Chem., Int. Ed.*, 2012, **51**, 3822–3825; (*b*) Q. G. Wang, Z. M. Yang, X. Q. Zhang, X. D. Xiao, C. K. Chang and B. Xu, *Angew. Chem., Int. Ed.*, 2007, **46**, 4285–4289; (*c*) M. Zhou, Y. Zhai and S. J. Dong, *Anal. Chem.*, 2009, **81**, 5603–5613.

11 (*a*) D. B. Lu, Y. Zhang, S. X. Lin, L. T. Wang and C. M. Wang, *Talanta*, 2013, **112**, 111–116; (*b*) S. Nandin, S. Nalini and G. S. Suresh, *J. Electroanal. Chem.*, 2013, **689**, 233–242; (*c*) H. C. Chang, X. M. Wang and H. Jiang, *Biosens. Bioelectron.*, 2013, **41**, 789–794; (*d*) F. Terzi, J. Pelliciari and R. Seeber, *Anal. Bioanal. Chem.*, 2013, **405**, 3579–3586.